

Influence of Gd^{3+} and Dy^{3+} co-doping and sintering regime on enhancement of electrical conductivity of ceria-based solid electrolyte

Z. Khakpour · A. A. Youzbashi · A. Maghsoudipour

Received: 14 October 2013 / Revised: 1 February 2014 / Accepted: 13 February 2014 / Published online: 15 March 2014
© Springer-Verlag Berlin Heidelberg 2014

Abstract In order to improve the conductivity of ceria-based solid electrolytes, effect of co-doped Gd^{3+} and Dy^{3+} was evaluated. For this purpose, nano-crystalline $Gd_{0.2-x}Dy_xCe_{0.8}O_{1.9}$ powders with various composition ranges ($x=0.05, 0.1, 0.15, 0.2$) were initially synthesized by high-energy milling method. The effect of micro-structural evolution and co-doping on electrical properties of the dense sintered samples fabricated by two-step sintering and conventional sintering of the synthesized powders were investigated. Electrical conductivity of the samples was discussed based on the results obtained by AC impedance spectroscopy at temperatures in the range of 300–700 °C. The co-doping and sintering regime were found to significantly influence the conductivity of the electrolytes. The electrical conductivity of the co-doped samples depends on Dy^{3+} content and the maximum conductivity obtained by 0.15 mol% Dy and 0.05 mol% Gd. The conductivity of $Gd_{0.2-x}Dy_xCe_{0.8}O_{1.9}$ ($x=0.15$) was 0.03 S/cm at 700 °C. A thorough discussion was made, based on the present experimental data.

Keywords Co-doping · Ceria-based electrolytes · Microstructure · Impedance spectroscopy

Introduction

Solid oxide fuel cells (SOFCs) are considered as the most efficient devices for direct conversion of chemical energy into electrical power [1]. Although their energy conversion efficiencies (45 to 60 %) are much higher than those of the conventional methods of power generation and produce minimal pollutant emissions, they have not been yet considered for wide commercial applications due to their higher cost. Lowering the operating temperature in SOFCs would appreciably reduce the costs as inexpensive refractory metals or ceramic components can be used. It would also ensure a greater overall system stability, reliability, efficiency, and a reduction in thermal stresses between the components in SOFCs, leading to a longer lifetime for the system [2, 3]. Therefore, development of new electrolyte materials with higher ionic conductivity at lower operation temperatures is the key factor for commercialization of SOFCs. Ceria-based oxides have been considered as the most promising solid electrolyte materials for use in IT-SOFCs [3–5]. These materials exhibit higher ionic conductivity at relatively lower temperatures in comparison to yttria-stabilized zirconia (YSZ) electrolytes, which could make them as suitable alternatives. Most of the studies carried out on ceria-based electrolytes focused mainly on improving electrical properties through optimizing the dopants kind and concentration [5–7], as well as their microstructure and sinter ability [8–10]. It is generally accepted that Gd^{3+} and Sm^{3+} doped ceria electrolytes exhibit the highest ionic conductivity as a result of the small association enthalpy between the dopant cations and oxygen vacancies [6, 7]. Further investigations towards enhancing the conductivity of ceria-based electrolytes have shown that the co-doping of certain cations can also be effective. The mechanism proposed for the observed improvement in electrical conductivity of the co-doped ceria is based on lowering the association enthalpy of oxygen vacancies and the dopant ions.

Z. Khakpour (✉) · A. Maghsoudipour
Ceramic Department, Materials and Energy Research Center,
P.O. Box 14155-4777, Tehran, Iran
e-mail: z-khakpour@merc.ac.ir

Z. Khakpour
e-mail: zahra_khakpour@yahoo.com

A. A. Youzbashi
Semiconductors Department, Materials and Energy Research Center,
P.O. Box 14155-4777, Tehran, Iran

According to Kilner and Brook [11], association enthalpy is minimum when there is no elastic strain in the host lattice. Omar et al. [12] attempted co-doping of Nd^{3+} and Lu^{3+} into ceria in order to find out the optimum radius that could result in lower strain and higher conductivity. However, the electrical property of ceria co-doped with Nd and Lu is poor, as compared to ceria doped with Gd, which indicates that the elastic energy is not the only factor to be considered. Recently, Omar et al. [13] evaluated the co-doping strategy (Nd/Sm) based on a density functional theory (DFT) to predict the interaction energy between the oxygen vacancies and the dopant cations [14]. Their results showed that the minimum elastic strain cannot properly explain the observed ionic conductivity in the co-doped ceria system under study. In fact, according to this theory, the interaction between dopants in crystal lattice constitutes the elastic repulsion as well as the electronic attraction [14]. Indeed, the most important aspect of this theory is the use of an appropriate mixture of dopants that could result in a constructive interaction of the elastic and electronic contributions improving the ionic conductivity. The co-doping may also increase the configurational entropy, modify the elastic strain in the crystal lattice, and change which the grain boundary composition.

Some co-doped ceria-based electrolyte systems such as $(\text{Ce}_{(1-x-y)}\text{La}_x\text{M}_y)\text{O}_{2-\delta}$ ($\text{M} = \text{Ca}, \text{Sr}$) [15, 16], $(\text{La}_{0.75}\text{Sr}_{0.2}\text{Ba}_{0.05})_{0.175}\text{Ce}_{0.825}\text{O}_{1.891}$ [17], $\text{Ce}_{1-x-y}\text{Sm}_x\text{Ca}_y\text{O}_{2-z}$ [18], $\text{Ce}_{0.8+x}\text{Y}_{0.2-2x}\text{Ca}_x\text{O}_{1.9}$ [19], $\text{Ce}_{1-a}\text{Gd}_{a-y}\text{Sm}_y\text{O}_{2-0.5a}$ [20], $\text{Ce}_{1-x-y}\text{Gd}_x\text{Pr}_y\text{O}_{2-z}$ [21], $\text{Ce}_{0.85}\text{Gd}_{0.1}\text{Mg}_{0.05}\text{O}_{1.9}$ [22], $\text{Ce}_{0.8}\text{Sm}_{0.2-x}\text{Y}(\text{La})_x\text{O}_{1.9}$ [23], $\text{Ce}_{0.8}\text{La}_{0.2-x}\text{Y}_x\text{O}_{1.9}$ [24], $\text{Ce}_{1-x}(\text{Sm}_{0.5}\text{Nd}_{0.5})_x\text{O}_\delta$ [25], $\text{Ce}_{0.8}\text{Gd}_{0.2-x}\text{Ca}_x\text{O}_{2-\delta}$ ($x=0-0.2$) [26], and so on [27–29] have been so far investigated.

In present study, the effect of Gd^{3+} and Dy^{3+} co-doping on electrical conductivity of ceria-based electrolytes was investigated. Since the ionic radius of Dy^{3+} (1.027 Å) is smaller than that of Gd^{3+} (1.053 Å) and slightly larger than that of Ce^{4+} (0.97 Å), the elastic strain in the crystal lattice could be expected to decrease. There are some reports on dysprosium-doped ceria electrolytes that have comparable association enthalpy values to those of samarium- or gadolinium-doped ceria electrolytes [9, 30]. Moreover, the microstructure of the sintered electrolytes, which is influenced by chemical composition and preparation method, has strong impact on the ionic conductivity. Enhanced grain boundary conductivity obtained by utilizing additives and modifying the microstructure using the appropriate sintering regime [31–33] which scavenge the impurity phases at the grain boundaries is still controversial. Our previous work [33] has shown that two-step sintering (TSS) is an effective way to fabricate dense ceramic electrolyte at lower temperatures. We have shown that TSS method can strongly affect the grain boundary conductivity in ceria-based electrolytes.

In this work, influence of co-doping and various sintering regimes (conventional sintering (CS) and TSS) were

evaluated. The composition and sintering conditions as regard to the total conductivity were optimized by investigating the effect of co-doping the Gd and Dy, their content, and sintering conditions on grain and grain boundary conductivities.

Experimental

The precursor materials used for the synthesis include CeO_2 , Gd_2O_3 , and Dy_2O_3 powder (Alfa Aesar with 99.99 % purity). They were placed into a planetary ball mill according to the stoichiometric formula of $\text{Gd}_{0.2}\text{Dy}_{0.2-x}\text{Ce}_{0.8}\text{O}_{1.9}$ ($x=0, 0.05, 0.1, 0.15, \text{ and } 0.2$). They were processed with a rotary speed of 270 rpm, a ball to powder weight ratio of 10:1 using zirconia vial (60 ml) and balls (10 and 20 mm diameters). Ball milling process was continued for up to 30 h. Details of the experiments were thoroughly explained in the previous paper [34].

Phase identification was performed by X-ray diffractometry (Philips) using $\text{CoK}\alpha$ radiation ($\lambda=1.78$ Å) as X-ray source, with step size of 0.02° and a step time of 2 s. Crystallite size of the fine powder products was estimated by Williamson–Hall method [35]. The lattice parameter (a) was determined by fitting the observed reflection with a least squares refinement program. The green compact pellets (13 mm in diameter and 1–2 mm in thickness) with a green density of about 64 % were prepared by pressing the ball milled powder at 500 MPa, and undergone the TSS process. In the first step, the pellets in static air were heated up to the higher temperature of $T_1=1,450$ °C, with a heating rate of 10 °C/min, after which they were cooled down to the lower temperature of $T_2=1,300$ °C with a cooling rate of 50 °C/min and held there for 20 h. For comparison, the compact bodies were also sintered conventionally at $1,500$ °C for 5 h with heating rate of 5 °C/min (CS). The bulk density of sintered pellets was determined using Archimedes method. The relative density of the sintered pellets was calculated from the ratio of bulk density to the density calculated from X-ray diffraction data. The average grain size of the sintered bodies was calculated using linear intercept method measured from at least 100 randomly selected grains recorded by SEM. To prepare the specimens for SEM analysis, the samples were polished and thermally etched at a temperature being $50-100$ °C lower than the sintering temperature.

To measure the electrical conductivity, platinum electrodes were applied on both sides of the sintered bodies of Pt paste coating, drying, and heat treating it at 600 °C for 1 h. Conductivities of the sintered bodies were measured by two-probe AC impedance spectroscopy (IS) at $400-700$ °C temperature and $0.1-10^6$ Hz frequency ranges.

Result and discussion

Synthesis and microstructure characterization

The structural impact of Dy and Gd co-doping was assessed by X-ray diffraction (XRD). Figure 1 shows the XRD profiles of the mixed CeO₂, Gd₂O₃, and Dy₂O₃ powders with appropriate proportions to obtain the compositions of Gd_{0.2}Ce_{0.8}O_{1.9}, Gd_{0.15}Dy_{0.05}Ce_{0.8}O_{1.9}, Gd_{0.1}Dy_{0.1}Ce_{0.8}O_{1.9}, Gd_{0.05}Dy_{0.15}Ce_{0.8}O_{1.9}, and Dy_{0.2}Ce_{0.8}O_{1.9} after 30 h ball milling. The XRD patterns were compared with the JCPDS files of CeO₂, Gd_{0.2}Ce_{0.8}O_{1.9}, Dy_{0.2}Ce_{0.8}O_{1.9}, and Dy₂O₃, respectively. It was found that all the milled products except Dy_{0.2}Ce_{0.8}O_{1.9} are single-phase materials with a cubic fluorite structure similar to pure CeO₂. The low intensity peak detected in XRD pattern of Dy_{0.2}Ce_{0.8}O_{1.9} (is arrowed in Fig. 1) at 2θ=30.80 can be related to the presence of Dy₂O₃ phase (JCPDC file no. 018-0475). The lattice parameter values were estimated for all the samples whose results are presented in Fig. 2. The results clearly indicate that the lattice parameter of Gd_{0.2}Ce_{0.8}O_{1.9} solid solution (5.419 Å) decreases linearly with increasing x, which satisfies Regard’s law due to the smaller radius of Dy⁺³ (r=1.027 Å) as compared to Gd⁺³ (r=1.053 Å). Observation of such trend could confirm the formation of the solid solution. Figure 3 shows the SEM micrograph of Gd_{0.15}Dy_{0.05}Ce_{0.8}O_{1.9} powder obtained after 30 h milling. The average crystallite size was calculated based on XRD results to be about 40 nm. This indicates that agglomeration of powder would occur as a result of the milling process and reduction in size.

Fig. 1 XRD profiles of Gd_{0.2}Ce_{0.8}O_{1.9}, Gd_{0.15}Dy_{0.05}Ce_{0.8}O_{1.9}, Gd_{0.1}Dy_{0.1}Ce_{0.8}O_{1.9}, Gd_{0.05}Dy_{0.15}Ce_{0.8}O_{1.9}, and Dy_{0.2}Ce_{0.8}O_{1.9} after 30 h milling. The secondary peak (arrowed) was indexed as Dy₂O₃. All other peaks belong to ceria fluorite structure

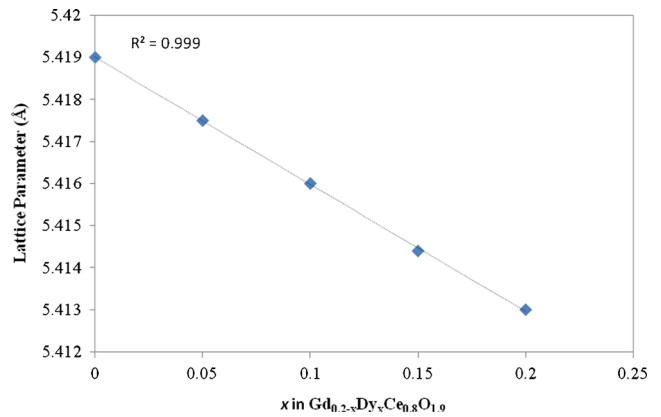
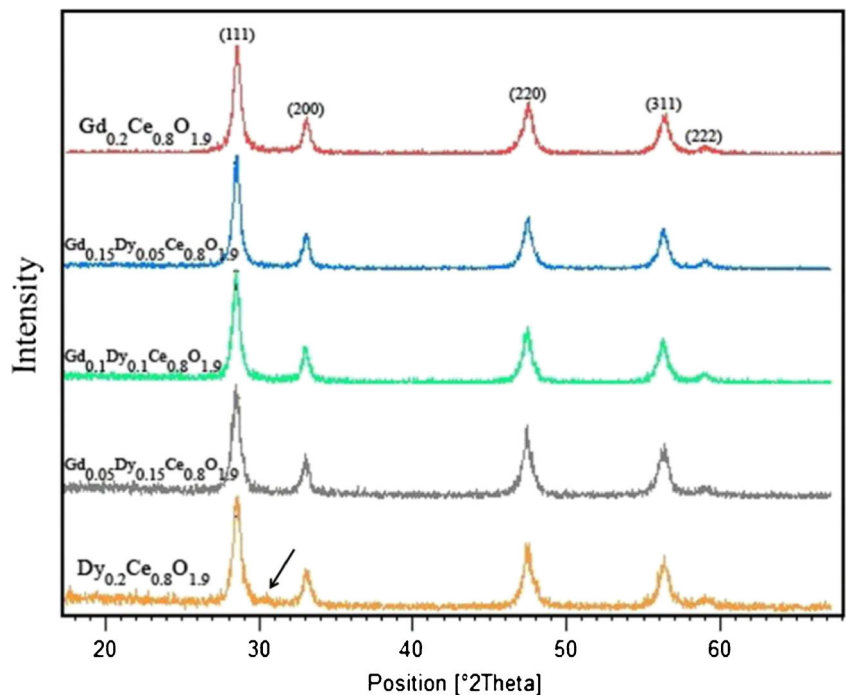


Fig. 2 Dependence of lattice parameter on the composition (x) of different doped ceria samples

Figure 4 shows SEM micrographs of polished and thermally etched surfaces of the ceramics sintered by the CS and TSS processes. The microstructures of the samples show the pentagonal and hexagonal grains without any intra-grain porosity. A grain size reduction in the case of TSS ceramics could be observed, which are more pronounced for the samples with 0.05 and 0.15 mol% Dy (Fig. 4a, c). The two-step sintering of these ceramics led to the formation of bodies with nearly full densities, i.e., >95 %. The estimated values of average grain size and relative density for doped and co-doped samples sintered under CS and TSS regimes by Gd and Dy dopants are given in Table 1. The relative densities of the co-doped ceramics normally sintered at 1,500 °C for 5 h were found to be more than 98 %. The relative density of singly Gd-doped ceria sintered under the same condition was found to be 92 %.

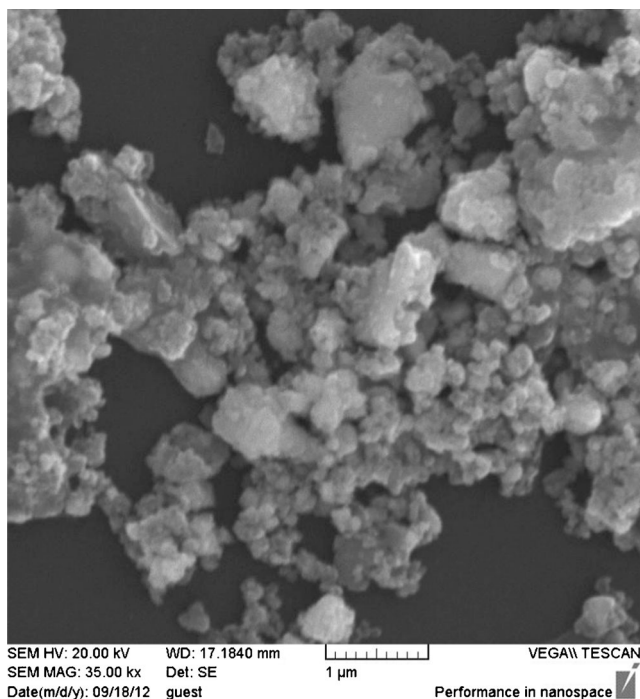


Fig. 3 SEM micrograph showing typical particle morphology of the synthesized $\text{Gd}_{0.15}\text{Dy}_{0.05}\text{Ce}_{0.8}\text{O}_{1.9}$ powder

Improved densification as a result of co-doping could be due to the decrease in Dy and Gd atomic migration to grain boundaries during the sintering process which could otherwise led to the solute drag phenomenon. Furthermore, the formation of liquid phase in the case of the conventionally sintered samples as a result of high temperature sintering can also be a reason for the improved densification.

The secondary phase (rod-shaped phase marked with circle in Fig. 4c) which was observed in the case of CS- $\text{Gd}_{0.05}\text{Dy}_{0.15}\text{Ce}_{0.8}\text{O}_{1.9}$ co-doped sample could not be detected by XRD analysis. This phase was also observed in CS $\text{Gd}_{0.15}\text{Dy}_{0.05}\text{Ce}_{0.8}\text{O}_{1.9}$ co-doped sample, but comparatively in lower amount. Formations of such secondary phases have been also reported elsewhere [36–38]. The results of the elemental analysis of the phases observed in SEM image of $\text{Gd}_{0.05}\text{Dy}_{0.15}\text{Ce}_{0.8}\text{O}_{1.9}$ co-doped sample are presented in Table 2. Based on the extensive SEM/EDS analyses, the secondary phase observed in this sample contains a higher concentration of Gd as compared to Ce and Dy along with minor amount of Si impurity. The presence of Si impurity in the secondary phase was also observed in our pervious works in singly doped ceria systems [33, 36]. Existence of such secondary phases at grain boundaries in the similar ceramic systems can behave as traps or produce some drags for migration of ions which may be responsible for conductivity, especially at the intermediate temperatures [39, 40]. However, if the secondary phase is formed at the cost of the disappearance of the siliceous glassy phase (or scavenging of Si) at

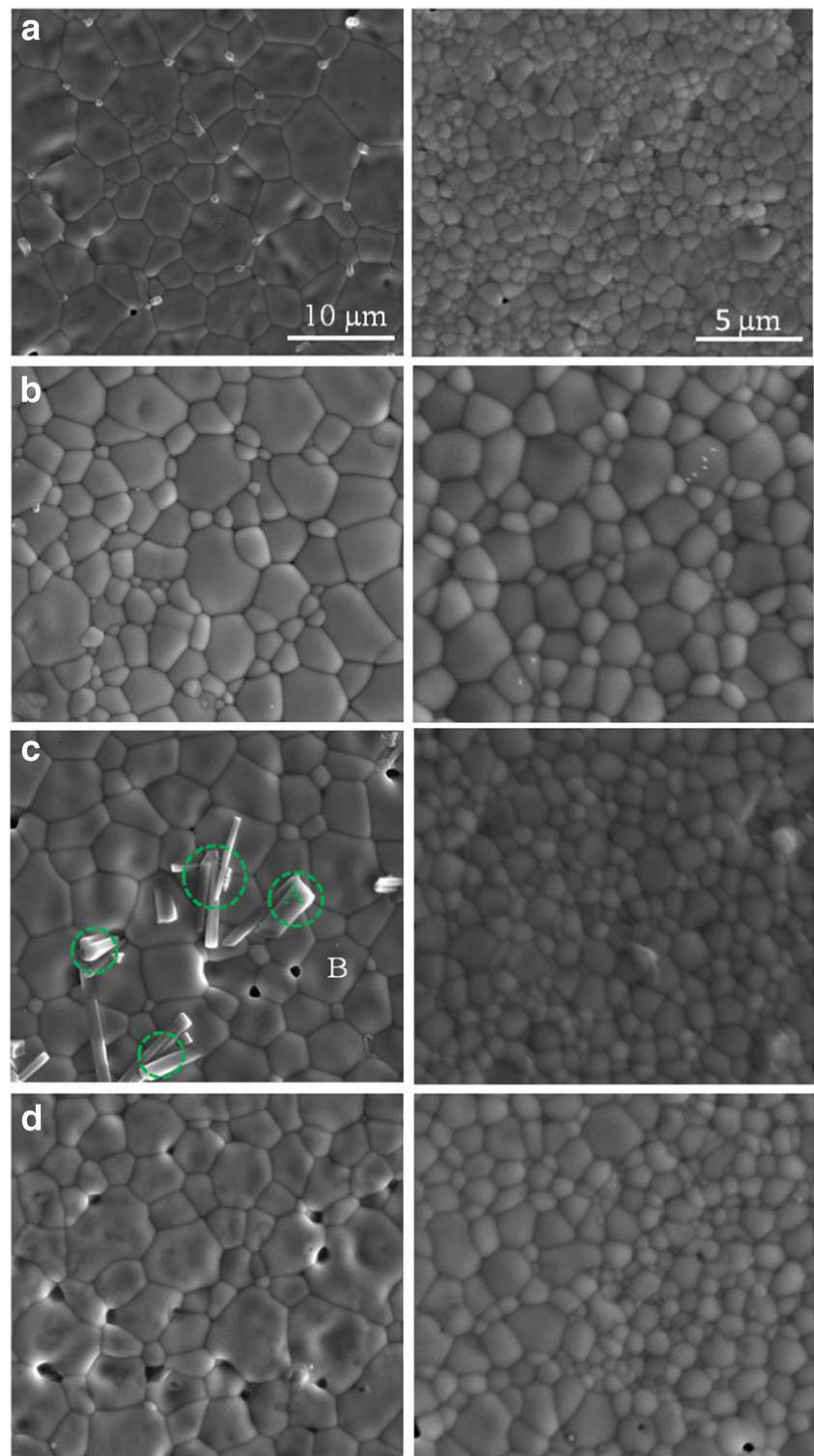
grain boundaries, it may promote the grain boundary conductivity [33].

Conductivities

For investigating the effect of the co-doping, total dopant concentration should be kept constant. In order to avoid the simultaneous effect of oxygen vacancy, the doping level was therefore kept at constant volume of 20 mol%. The ac impedance spectroscopy was used to evaluate the electrical properties of the high density sintered singly doped and co-doped pellets fabricated by CS and TSS processing. The impedance spectra and equivalent circuit model of CS- $\text{Gd}_{0.05}\text{Dy}_{0.15}\text{Ce}_{0.8}\text{O}_{1.9}$ electrolyte at 300 °C are shown in Fig. 5. The impedance spectra were fitted by means of an equivalent electrical circuit consisting of a series of three sub-circuits of parallel resistors–CPE elements. The sub-circuits were attributed to bulk (lattice), grain boundary dispersion as well as the electrode/electrolyte inter-phase. The frequency increases from right to left across the plot. After fitting the obtained values for the bulk (high frequency) and grain boundary (intermediate frequency), the resistance values were converted into lattice and grain boundary conductivities. The impedance spectra of CS and TSS- $\text{Gd}_{0.2-x}\text{Dy}_x\text{Ce}_{0.8}\text{O}_{1.9}$ electrolytes with $x=0, 0.05, 0.1, 0.15,$ and 0.2 at 400 °C are shown in Fig. 6, where three main features similar to Fig. 5 can be observed. Two distinct arcs were detected at high frequencies and incomplete one at lower frequencies.

In Fig. 6, the impedance spectra have been normalized to the sample geometry (A , surface area; t , thickness). The normalized capacitances for different composition are in the range of 10^{-9} to 10^{-7} F/cm for the high frequency contribution (the bulk contribution) and 10^{-7} to 10^{-5} F/cm for the intermediate frequency term (the grain boundary contribution). Capacitance values were estimated by the constant phase element from the $1/RC$ relationship [41]. C_b and C_{gb} were calculated to be in the same order of magnitude reported for the doped ceria-based electrolyte ($C_{gb} \gg C_b$) [42]. From Fig. 6, it can be seen that ceria co-doped with Gd and Dy with $x=0.15$ ($\text{Gd}_{0.05}\text{Dy}_{0.15}\text{Ce}_{0.8}\text{O}_{1.9}$) exhibits the highest bulk and grain boundary conductivity (which is about 1.4×10^{-3} and $9.0 \times 10^{-4} \text{ Scm}^{-1}$ at 400 °C). The results are related to the TSS and CS regimes. The co-doped sample with Dy and Gd with $x=0.1$ exhibits the highest grain boundary resistivity when conventionally sintered (CS). The highest grain boundary resistivity at 400 °C for CS samples belongs to singly Dy-doped ceria electrolyte. In TSS samples, ceria co-doped with Dy and Gd with $x=0.1$ exhibits the highest bulk resistivity; however, the highest grain boundary resistivity belongs to Gd singly doped ceria sample.

Fig. 4 Microstructures of polished and thermally etched surface of **a** $\text{Gd}_{0.15}\text{Dy}_{0.05}\text{Ce}_{0.8}\text{O}_{1.9}$; **b** $\text{Gd}_{0.1}\text{Dy}_{0.1}\text{Ce}_{0.8}\text{O}_{1.9}$; **c** $\text{Gd}_{0.05}\text{Dy}_{0.15}\text{Ce}_{0.8}\text{O}_{1.9}$; **d** $\text{Dy}_{0.2}\text{Ce}_{0.8}\text{O}_{1.9}$, conventional sintering (CS) at 1,500 °C for 5 h (*right*) and TSS (*left*). The notation in Fig. 3 (c) indicated secondary Gd-rich phase determined by EDS analysis



The sintering regime clearly influences the resistivity (Fig. 6). Particularly, the $\text{Gd}_{0.15}\text{Dy}_{0.05}\text{Ce}_{0.8}\text{O}_{1.9}$ electrolyte which has been sintered with TSS regime behaves clearly different from the same composition with CS regime. TSS regime leads to reduction in the bulk and grain boundary resistivity in this electrolyte at 400 °C. Among the reports

for singly Dy^{3+} -doped ceria [9, 29, 39], Mori et al. [40] reported that combination of spark plasma sintering and conventional sintering methods increased its conductivity. They believed that by optimizing the microstructure and grain size, conductivity in Dy-doped CeO_2 electrolytes could be effectively improved. It can be seen from Fig. 6 that the grain and

Table 1 Sintering condition, green and totally relative density and grain size of doped and co-doped samples obtained by CS and TSS methods

Composition	CS				TSS			
	ρ_0 (%)	T (°C)	ρ_t (%)	Grain size (μm)	T_1 (°C)	T_2 (°C)	ρ_t (%)	Grain size (nm)
Gd _{0.2} Ce _{0.8} O _{1.9}	60	1,500	92	6	1,450	1,300	99.5	1,100
Gd _{0.15} Dy _{0.05} Ce _{0.8} O _{1.9}	60	1,500	98.5	3.8	1,450	1,300	98	600
Gd _{0.1} Dy _{0.1} Ce _{0.8} O _{1.9}	60	1,500	98	3.5	1,450	1,300	98	1,100
Gd _{0.05} Dy _{0.15} Ce _{0.8} O _{1.9}	60	1,500	99.5	4	1,450	1,300	99	700
Dy _{0.2} Ce _{0.8} O _{1.9}	60	1,500	98	3.5	1,450	1,300	95	1,000

grain boundary conductivities in Dy singly doped electrolyte were evidently enhanced by using the TSS regime.

The Arrhenius plots of grain, grain boundary, and total conductivities of the TSS and CS samples as a function of the testing temperature are shown in Figs. 7, 8, and 9, respectively. Figure 7 shows the grain conductivity of TSS and CS-Gd_{0.2-x}Dy_xCe_{0.8}O_{1.9} ($x=0, 0.05, 0.1, 0.15,$ and 0.2) electrolytes. It can be observed that the TSS and CS co-doped ceria with $x=0.15$ exhibit the highest grain conductivity among the all temperature ranges studied, and as the temperature is reduced (<500 °C), the differences in conductivities are increased. It is revealed in all the samples that use of any sintering regime give rise to different grain conductivity, except in the case of CS-Gd_{0.05}Dy_{0.15}Ce_{0.8}O_{1.9} sample.

Co-doping effect has been also discussed in terms of the configurational entropy [30]. Yamamura et al. [43] indicated that the co-doping could suppress the ordering of the oxygen vacancy and lowering the activation energy of conduction. In the next step, the activation energy (enthalpy) of the ionic motion (ΔE) in lattice (bulk) and total (bulk and grain boundary) were calculated using line slopes. The intercept of the plot with $\ln\sigma T$ axis (for $1000/T \rightarrow 0$) was used to calculate the pre-exponential factor (σ_0). The obtained results reveal that the increment of the configurational entropy as a result of co-doping is not the dominant factor responsible for increasing the grain conductivity. For instance, in contrast to the singly doped ceria electrolytes, although the configurational entropy increased in co-doped samples with 0.1 mol% Dy increases, conductivity was found to decrease. Therefore, it may be concluded that the activation energy of the bulk conduction could be more dominant. It can be seen from Table 3 that the

Table 2 The compositions (atomic %) of the secondary phase and matrix in Fig. 4c are listed for CS-Gd_{0.05}Dy_{0.15}Ce_{0.8}O_{1.9} obtained using the energy dispersive spectroscopy (EDS) analysis

Element	Secondary phase	Matrix
Ce	54.08	80.39
Gd	31.08	4.65
Dy	13.26	15.06
Si	1.23	–

lowest activation energy of the bulk conduction belongs to the TSS and CS-Gd_{0.05}Dy_{0.15}Ce_{0.8}O_{1.9} and also TSS-Gd_{0.15}Dy_{0.05}Ce_{0.8}O_{1.9} electrolytes. Therefore, the electrical conductivity strongly depends on Dy³⁺ contents. Omar et al. [13] studied the relationship between the elastic strain and ionic conductivity in doped ceria compounds and found that the ionic conductivity is not specifically the function of the lattice deviation in doped ceria electrolytes. In this work, Nd³⁺ was chosen as a dopant based on the DFT work performed by Anderson et al. [14] which exhibited the highest grain ionic conductivity among all other doped ceria materials. In the present study, Gd³⁺ and Dy³⁺ co-doped samples have a weighted average dopant radii of 1.045, 1.04, and 1.033 Å for $x=0.05, 0.1,$ and 0.15 mol% Dy, respectively. The weighted average dopant radius at $x=0.1$ is closer to the r_c value (1.038 Å) determined by Kim [44]. Nevertheless, the grain ionic conductivity of Gd_{0.1}Dy_{0.1}Ce_{0.8}O_{1.9} is less than other samples. However, increasing the radius value has lowered the activation energy of conduction in the Gd_{0.05}Dy_{0.15}Ce_{0.8}O_{1.9} and Gd_{0.15}Dy_{0.05}Ce_{0.8}O_{1.9} samples as Anderson reported [14].

Figure 8 indicates the grain boundary conductivity of TSS and CS-Gd_{0.2-x}Dy_xCe_{0.8}O_{1.9} ($x=0, 0.05, 0.1, 0.15,$ and 0.2) electrolytes. The highest grain boundary conductivity belongs to CS and TSS co-doped ceria with $x=0.15$ and TSS co-doped ceria with $x=0.05$. No clear transition points in these curves

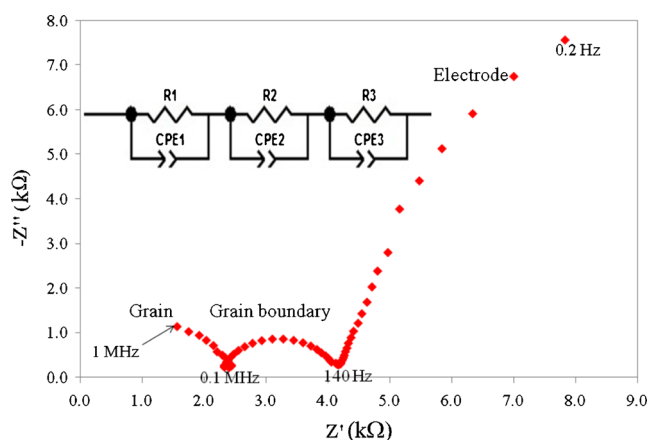
**Fig. 5** Complex impedance spectra and equivalent circuit model of Gd_{0.05}Dy_{0.15}Ce_{0.8}O_{1.9} electrolyte at 300 °C

Fig. 6 Complex impedance plots of CS and TSS $Gd_{0.2-x}Dy_xCe_{0.8}O_{1.9}$ ($x=0, 0.05, 0.1, 0.15,$ and 0.2) ceramics with annealed Pt paste electrodes measured at $400\text{ }^\circ\text{C}$ using two-probe technique. High frequency part of the CS ceramics spectrum is shown in the insert

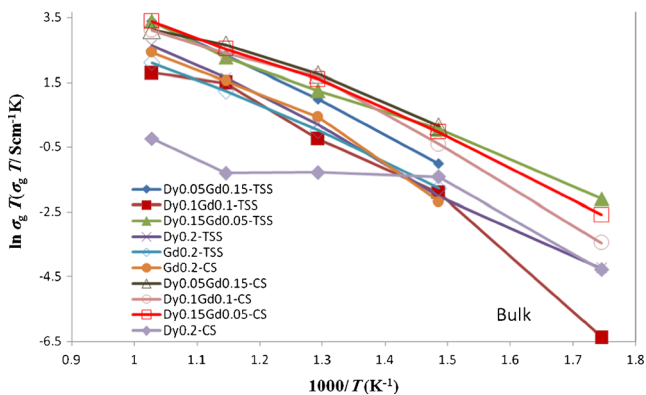
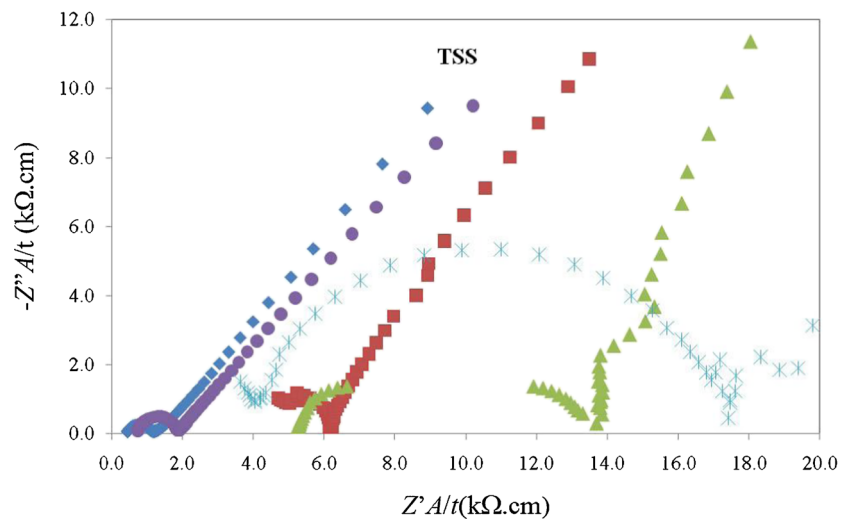
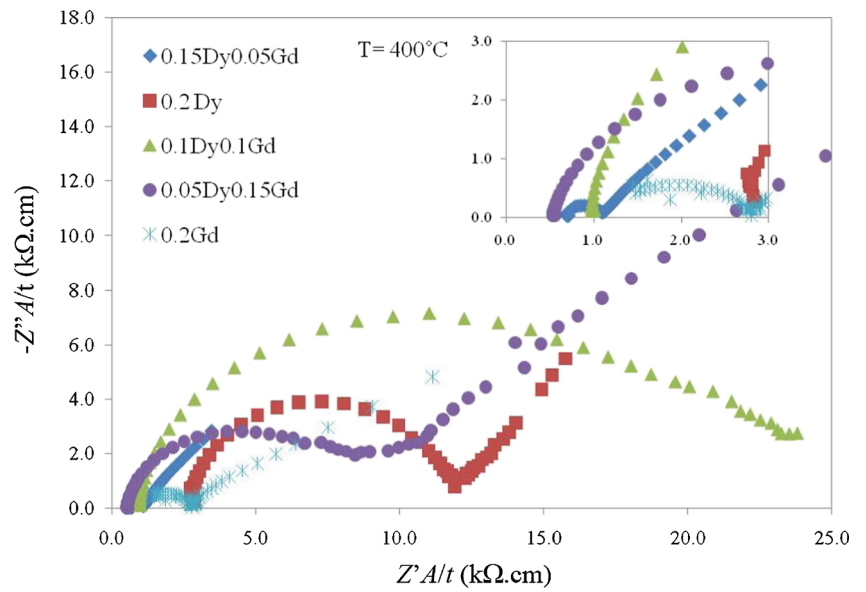


Fig. 7 Arrhenius type plots of bulk conductivity for CS and TSS $Gd_{0.2-x}Dy_xCe_{0.8}O_{1.9}$ electrolytes with $x=0, 0.05, 0.1, 0.15,$ and $0.2,$ and different grain size

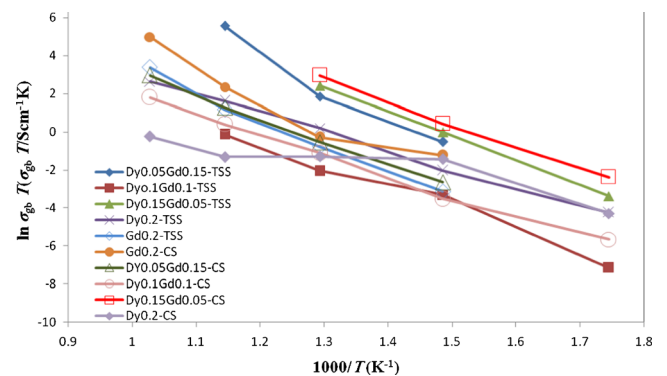


Fig. 8 Arrhenius type plots of grain boundary conductivity for CS and TSS $Gd_{0.2-x}Dy_xCe_{0.8}O_{1.9}$ electrolytes with $x=0, 0.05, 0.1, 0.15,$ and $0.2,$ and different grain size

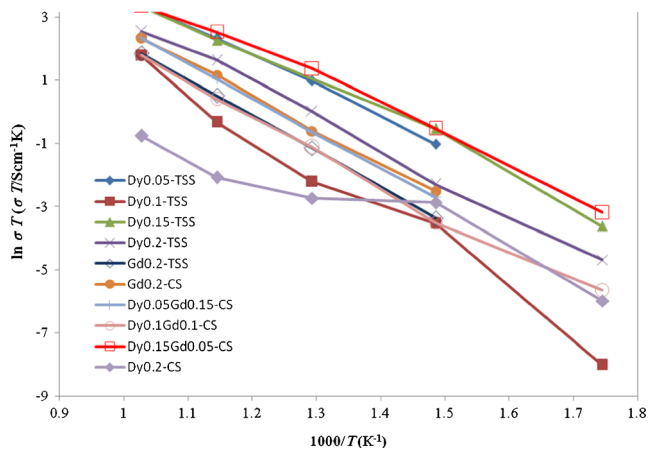


Fig. 9 Arrhenius-type plots of total conductivity for CS and TSS $Gd_{0.2-x}Dy_xCe_{0.8}O_{1.9}$ electrolytes with $x=0, 0.05, 0.1, 0.15,$ and $0.2,$ and different grain size

were found which is attributed to remarkable increment in temperature measurement ($100\text{ }^\circ\text{C}$). However, as observed in Figs. 7 and 8, the increase in conductivity in the temperature range of $400\text{--}500\text{ }^\circ\text{C}$ is more pronounced. Results show that the lowest conductivity was obtained in co-doped ceria with $x=0.1$ and singly doped ceria with Dy. TSS regime can improve the conductivity of the singly doped Dy but in co-doped sample ($x=0.1$) it acts in the opposite way. As it was discussed earlier, the relative density of any CS composition is almost the same, so the enhancement of grain boundary conductivity primarily depends on the composition. Grain boundaries play the major role in overall conductivity in the investigated temperature range.

The grain boundary resistance in ceria-based electrolytes is created by two main factors: (1) the grain boundary impurity or glassy phase that blocks the ionic transport across the boundaries by decreasing the conduction path width and constricting the current lines, the phenomenon which is called

extrinsic effect, and (2) intrinsic effect which is due to the space charge layer at grain boundaries [39]. It leads to a situation where the oxygen vacancies are severely depleted and subsequently the grain boundary conductivity would be decreased. Therefore, the excess of aliovalent elements segregating at grain boundaries can result in lower grain boundary conductivity at the same doping level. As it was shown, the secondary Si and dopant (Gd) rich phase in CS-singly or co-doped samples could be detected in $Gd_{0.05}Dy_{0.15}Ce_{0.8}O_{1.9}$ sample. It seems that scavenging of Si at grain boundary by formation of secondary phase in that sample results in lowering the deterioration effect of Si glassy phase on the grain boundary conductivity. Owing to remove concentrated dopant cations from grain boundary regions, the formation of dopant-rich phase leads to the improvement of grain boundary conductivity. This phenomenon was also reported in our recently published work [33]. In Table 3, the total conductivity for different grain sizes have been compared. For better comparison, it should be better to separate the effects of true changes in grain boundary conductivity from those related to changes in grain sizes. With assumption that the brick layer model is the major factor responsible for the grain boundary resistivity, the specific grain boundary conductivity σ_{gb}^{sp} should be estimated that is related to the geometry of the grain boundary. Haile et al. [31] suggested that the capacitances of approximate value of σ_{gb}^{sp} could be calculated from the ratio of the bulk and grain boundary capacitances under the following assumptions: (I) a brick layer model, (II) $\sigma_{gb}^{sp} \ll \sigma_{bulk}$, (III) grain size \gg grain boundary thickness (δ_{gb}), (IV) permittivity of grain boundary phase (ϵ_{gb}) \cong permittivity of bulk phase according to the following equation:

$$\sigma_{gb}^{sp} \approx \frac{L}{R_{gb}A} \frac{C_{bulk}}{C_{gb}} \quad (1)$$

Table 3 Total conductivity, conductivity activation energies, and pre-exponential terms of the CS and TSS $Gd_{0.2-x}Dy_xCe_{0.8}O_{1.9}$ ($x=0, 0.05, 0.1, 0.15,$ and 0.2) electrolyte ceramics

Electrolytes	σ_{700t} (Scm^{-1})	σ_{400t} (Scm^{-1})	σ_{500t} (Scm^{-1})	σ_0 (Scm^{-1}K)	ΔE (eV)	ΔE_b (eV)	$\Delta \varphi_{400}$ (V)	$\Delta \varphi_{500}$ (V)	Grain size (μm)
CS- $Gd_{0.2}Ce_{0.8}O_{1.9}$	0.011	0.0001	0.0009	5.1×10^5	0.96	0.64	0.30	0.30	1.7
TSS- $Gd_{0.2}Ce_{0.8}O_{1.9}$	0.008	0.00005	0.0004	7.5×10^5	0.97	–	0.30	0.31	1.1
CS- $Gd_{0.15}Dy_{0.05}Ce_{0.8}O_{1.9}$	0.011	0.0001	0.0007	8.7×10^5	0.95	0.61	0.31	0.32	3.8
TSS- $Gd_{0.15}Dy_{0.05}Ce_{0.8}O_{1.9}$	0.03	0.0005	0.0034	7.5×10^5	0.82	0.59	0.22	0.22	0.69
CS- $Gd_{0.1}Dy_{0.1}Ce_{0.8}O_{1.9}$	0.006	0.000043	0.0002	2.6×10^5	1.08	0.79	0.40	0.40	3.5
TSS- $Gd_{0.1}Dy_{0.1}Ce_{0.8}O_{1.9}$	0.006	0.00004	0.0001	2.6×10^6	1.06	0.73	0.38	0.39	1.54
CS- $Gd_{0.05}Dy_{0.15}Ce_{0.8}O_{1.9}$	0.03	0.0009	0.005	4.6×10^5	0.79	0.59	0.19	0.18	4
TSS- $Gd_{0.05}Dy_{0.15}Ce_{0.8}O_{1.9}$	0.03	0.0009	0.0047	5.7×10^5	0.82	0.58	0.19	0.19	0.8
CS- $Dy_{0.2}Ce_{0.8}O_{1.9}$	0.00048	0.00006	0.0008	546.7	–	–	0.25	0.25	3.55
TSS- $Dy_{0.2}Ce_{0.8}O_{1.9}$	0.01	0.00015	0.0013	6.1×10^5	0.89	0.84	0.19	0.18	1.0

where C_{bulk} and C_{gb} are the capacitances of the bulk and grain boundary. These values derived from the impedance spectrum. With the specific grain boundary conductivity and the bulk conductivity, the Schottky barrier height, $\Delta\varphi_0$, can be calculated from Eq. (2):

$$\frac{\sigma_b}{\sigma_{\text{gb}}^{\text{SP}}} = \frac{\exp(2e\Delta\varphi_0/KT)}{4e\Delta\varphi_0/KT} \quad (2)$$

Where σ_b is the bulk conductivity, $\sigma_{\text{gb}}^{\text{SP}}$ is the specific grain boundary conductivity, and $\Delta\varphi_0$ is Schottky barrier height. $\Delta\varphi_0$ can be used to describe the depletion of electron holes in the space charge layer [39]. The values of $\Delta\varphi_0$ (Schottky barrier height) at 400 and 500 °C for the doped and co-doped ceramics are summarized in Table 3. It can be seen that co-doped $\text{Gd}_{0.05}\text{Dy}_{0.15}\text{Ce}_{0.8}\text{O}_{1.9}$ and TSS- $\text{Gd}_{0.15}\text{Dy}_{0.05}\text{Ce}_{0.8}\text{O}_{1.9}$ electrolytes exhibit the lowest Schottky barrier height values ($\Delta\varphi_0=0.19$ and 0.22 V at 400 °C). The highest Schottky barrier height belongs to the co-doped TSS and CS- $\text{Gd}_{0.1}\text{Dy}_{0.1}\text{Ce}_{0.8}\text{O}_{1.9}$ electrolytes (0.38 and 0.39 V at 400 °C).

Guo and Waser [39] reported that in Y_2O_3 -doped ZrO_2 electrolytes, when $\Delta\varphi_0$ is very high (e.g., 0.35 V), the space charge effect can be always dominant in the grain boundary resistance. In that case, results show that the space charge effect is dominant in TSS and CS- $\text{Gd}_{0.1}\text{Dy}_{0.1}\text{Ce}_{0.8}\text{O}_{1.9}$ at 400 and 500 °C. As reported [8, 38], a small amount of SiO_2 markedly increases the grain boundary resistance too. Guo and Waser [39] indicated that for such situation, a much high coverage of grain boundaries by siliceous phase is required. This situation is detected in materials of normal purity. However, in materials of high purity, the oxygen vacancy depletion in the space-charge layer accounts for the grain boundary electrical conductivity. Since the Schottky barrier height quantities in co-doped $\text{Gd}_{0.05}\text{Dy}_{0.15}\text{Ce}_{0.8}\text{O}_{1.9}$ and TSS- $\text{Gd}_{0.15}\text{Dy}_{0.05}\text{Ce}_{0.8}\text{O}_{1.9}$ electrolytes are low, the grain boundary resistivity can be concluded to be intrinsic.

According to the obtained results, it can be noted that co-doped Gd/Dy composition and sintering regime can individually influence on the grain boundary conductivity. The higher grain boundary conductivity in TSS- $\text{Gd}_{0.05}\text{Dy}_{0.15}\text{Ce}_{0.8}\text{O}_{1.9}$ and $\text{Gd}_{0.15}\text{Dy}_{0.05}\text{Ce}_{0.8}\text{O}_{1.9}$ electrolytes indicated that two-step sintering and co-doping strategy lead to the minor concentration of segregation dopants at grain boundary regions. In addition, finer grain-sized TSS materials leads to discontinuity of coverage the silicon-rich phase in the grain boundary regions. The formation of stable and discrete Si-containing phases at the grain boundary regions, dewetting of siliceous inter-granular liquid phase, the change in the space charge layer, and the change in the segregation and inter-phase structure were found to be the major factors affecting the grain

Table 4 Ionic conductivity of some studied co-doped electrolyte-based ceria at 500 °C

Sample	$\sigma_{500\text{t}}$ (Scm^{-1})	
TSS- $\text{Gd}_{0.15}\text{Dy}_{0.05}\text{Ce}_{0.8}\text{O}_{1.9}$	0.0034	In the present study
CS- $\text{Gd}_{0.05}\text{Dy}_{0.15}\text{Ce}_{0.8}\text{O}_{1.9}$	0.005	In the present study
CS- $\text{Gd}_{0.05}\text{Dy}_{0.15}\text{Ce}_{0.8}\text{O}_{1.9}$	0.0047	In the present study
$\text{Ce}_{0.85}\text{Gd}_{0.75}\text{Y}_{0.75}\text{O}_{1.925}$	0.004	[26]
$\text{Ce}_{0.85}\text{Gd}_{0.75}\text{Y}_{0.75}\text{O}_{1.925}$	0.003	[26]
$\text{Ce}_{0.85}\text{Gd}_{0.75}\text{Nd}_{0.75}\text{O}_{1.925}$	0.002	[26]
$\text{Gd}_{0.1}\text{Sm}_{0.05}\text{Ce}_{0.85}\text{O}_{1.925}$	0.0046	[18]
$\text{Gd}_{0.05}\text{Sm}_{0.1}\text{Ce}_{0.85}\text{O}_{1.925}$	0.0035	[18]
$\text{Ca}_{0.05}\text{Y}_{0.1}\text{Ce}_{0.85}\text{O}_{1.925}$	0.006	[21]
$\text{Ce}_{0.9}(\text{Sm}_{0.5}\text{Nd}_{0.5})\text{O}_{1.95}$	0.004	[23]
$\text{Y}_{0.1}\text{Sm}_{0.1}\text{Ce}_{0.8}\text{O}_{1.9}$	0.005	[24]

boundary conductivity. The collection of a Si-containing phase into discrete configuration by pre-sintering heat treatment in YSZ [45], YbSZ [46], and Gd-doped ceria [32] electrolytes have been reported earlier. In the case of co-doped CS- $\text{Gd}_{0.15}\text{Dy}_{0.05}\text{Ce}_{0.8}\text{O}_{1.9}$ electrolytes, it seems that the secondary phase has been formed during the sintering process. The dewetting of the inter-granular phase as a result of the crystallization of the secondary phase can be effective in reducing the effect of harmful siliceous phase at the grain boundary.

The ionic conductivity of the co-doped TSS and CS- $\text{Gd}_{0.05}\text{Dy}_{0.15}\text{Ce}_{0.8}\text{O}_{1.9}$ and TSS- $\text{Gd}_{0.15}\text{Dy}_{0.05}\text{Ce}_{0.8}\text{O}_{1.9}$ electrolytes at 500 °C are presented in Table 4 together with several other co-doped ceria-based ceramics for comparison. It is clear that the ionic conductivity for the currently co-doped (Gd-Dy) ceria is close to those obtained by some co-doped ceria electrolytes (e.g., $\text{Y}_{0.1}\text{Sm}_{0.1}\text{Ce}_{0.8}\text{O}_{1.9}$ and $\text{Gd}_{0.1}\text{Sm}_{0.05}\text{Ce}_{0.85}\text{O}_{1.925}$) and surpasses some of them in terms of ionic conductivity.

Conclusions

The effect of co-doping and sintering conditions (CS and TSS regime) on grain and grain boundary conductivity of ceria co-doped electrolyte with Dy^{3+} and Gd^{3+} was investigated. The results revealed that the co-doped electrolytes with an appropriate proportion of Dy^{3+} and Gd^{3+} (0.15 and 0.05 %mol) could have higher conductivity than singly doped ceria with the equal oxygen vacancy concentration. The co-doping as well as the sintering regime has influenced the electrical conductivity of grain boundary which leads to enhanced conductivity at intermediate temperature in co-doped $\text{Gd}_{0.05}\text{Dy}_{0.15}\text{Ce}_{0.8}\text{O}_{1.9}$ electrolyte.

References

- Singhal SL, Kendall K (2003) High temperature solid oxide fuel cells: fundamental, design and applications. Elsevier, Oxford
- Minh NQ (1993) Ceramic fuel cells. *J Am Ceram Soc* 76:563–588
- Steele BCH (2000) Materials for IT-SOFC stacks: 35 years R&D: the inevitability of gradualness? *Solid State Ionics* 134:3–20
- Inaba H, Tagawa H (1996) Ceria-based solid electrolytes. *Solid State Ionics* 83:1–16
- Yashiro H, Eguchi K, Arai H (1989) Electrical properties and reducibilities of ceria-rare earth oxide and their application to solid oxide fuel cell. *Solid State Ionics* 36:71–75
- Steele BCH (2000) Appraisal of $Ce_{1-y}Gd_yO_{2-y/2}$ electrolytes for IT-SOFC operation at 500 °C. *Solid State Ionics* 129:95–110
- Gerhardt-Anderson SR, Nowick AS (1981) Ionic conductivity of CeO_2 with trivalent dopants of different ionic radii. *Solid State Ionics* 5:547–550
- Tian C, Chan SW (2000) Ionic conductivities, sintering temperatures and microstructures of bulk ceramic CeO_2 doped with Y_2O_3 . *Solid State Ionics* 134:89–102
- Mori T, Buchanan B, Ou DR, Ye F, Kobayashi T, Kim JD, Zou J, Drennan J (2008) Design of nanostructured ceria-based solid electrolytes for development of IT-SOFC. *J Solid State Electrochem* 12: 841–849
- Lapa CM, de Souza DPF, Figueiredo FML, Marques FMB (2010) Two-step sintering ceria-based electrolytes. *Int J Hydrog Energy* 35: 2737–2741
- Kilner JA, Brook RJ (1982) A study on oxygen ion conductivity in doped non-stoichiometric oxides. *Solid State Ionics* 6: 237–252
- Omar S, Wachsman ED, Nino JC (2006) A co-doping approach towards enhanced ionic conductivity in fluorite-based electrolytes. *Solid State Ionics* 177:3199–3208
- Omar S, Wachsman ED, Jones JL, Nino JC (2009) Crystal structure-ionic conductivity relationships in doped ceria systems. *J Am Ceram Soc* 92:2674–2681
- Anderson DA, Simak SI, Skorodumova NV, Abrikosov IA, Johansson B (2006) Optimization of ionic conductivity in doped ceria. *Proc Natl Acad Sci U S A* 103:3528–3521
- Zheng Y, Shi Y, Gu H, Gao L, Chen H, Guo L (2009) La and Ca co-doped ceria-based electrolyte materials for IT-SOFCs. *Mater Res Bull* 44:1717–1721
- Jaiswal N, Upadhyay S, Kumar D, Parkash O (2013) Ionic conductivity investigation in lanthanum (La) and strontium (Sr) co-doped ceria system. *J Power Sources* 222:230–236
- Pikalova EY, Maragou VI, Demina AN, Demin AK, Tsiakaras PE (2008) The effect of co-dopant addition on the properties of $Ln_{0.2}Ce_{0.8}O_{2-\delta}$ ($Ln = Gd, Sm, La$) solid-state electrolyte. *J Power Sources* 181:199–206
- Mori T, Yamamura H (1998) Preparation of alkali-elements or alkali-earth-element-doped $CeO_2-Sm_2O_3$ system and its operation properties as the electrolyte in planar solid oxide fuel cells. *J Mater Synth Process* 6:175–179
- Homgemi X, Hongge Y, Zhenhua C (2008) Preparation and properties of Y^{3+} and Ca^{2+} co-doped ceria electrolyte materials for ITSOFC. *Solid State Sci* 10:1179–1184
- Wang FY, Chen S, Cheng S (2004) Gd^{3+} and Sm^{3+} co-doped ceria based electrolytes for intermediate temperature solid oxide fuel cells. *Electrochem Commun* 6:743–756
- Lubke S, Wiemhofer HD (1999) Electronic conductivity of Gd-doped ceria with additional Pr-doping. *Solid State Ionics* 117:229–243
- Wang F, Chen SY, Wang Q, Yu S, Cheng S (2004) Study on Gd and Mg co-doped ceria electrolyte for intermediate temperature solid oxide fuel cell. *Catal Today* 97:189–194
- Dudek M, Bogusz W, Zych L, Trybalska B (2008) Electrical and mechanical properties of CeO_2 -based electrolytes in the $CeO_2-Sm_2O_3-M_2O_3$ ($M = La, Y$) system. *Solid State Ionics* 197: 164–167
- Yoshida H, Deguchi H, Miura K, Horiuchi M, Inagak T (2001) Investigation of the relationship between the ionic conductivity and the local structures of singly and doubly doped ceria compounds using EXAFS measurement. *Solid State Ionics* 140:191–199
- Li B, Liu Y, Wei X, Pan W (2010) Electrical properties of ceria Co-doped with Sm^{3+} and Nd^{3+} . *J Power Sources* 195:969–976
- Zhao XL, Liu JJ, Xiao T, Wang JC, Zhang YX, Yao HC, Wang JS, Li ZJ (2012) Effect of Ca co-dopant on the electrical conductivity of Gd-doped ceria. *J Electroceram* 28:149–157
- Cheng J, Jiang Q, He H, Yang J, Wang Y, Gao J (2011) Preparation and characterization of $Y_2O_3-Sm_2O_3$ co-doped ceria electrolyte for IT-SOFCs. *Mater Chem Phys* 125:704–708
- Kim J, Lee D (2002) The effect of multiple doping on electrical conductivity of gadolinia-doped ceria electrolyte. *Korean J Chem Eng* 19:421–424
- Zajac W, Molenda J (2008) Electrical conductivity of doubly doped ceria. *Solid State Ionics* 179:154–158
- Acharya SA (2010) The effect of processing route on sinter ability and electrical properties of nano-sized dysprosium-doped ceria. *J Power Sources* 198:105–111
- Haile SM, West DL, Campbell J (1998) The role of the microstructure and processing on the proton conducting properties of gadolinium-doped barium cerate. *J Mater Res* 13:1576–1595
- Suk Kim D, Seok Cho P, Heun Lee J, Yeon Kim D, Lee SB (2006) Improvement of grain-boundary conduction in gadolinia-doped ceria via post-sintering heat treatment. *Solid State Ionics* 177:2125–2128
- Khakpour Z, Youzbashi AA, Maghsoudipour A, Ahmadi K (2012) Electrical conductivity of Sm-doped CeO_2 electrolyte produced by two-step sintering. *Solid State Ionics* 227:80–85
- Khakpour Z, Youzbashi AA, Maghsoudipour A, Ahmadi K (2011) Synthesis of nano sized gadolinium doped ceria solid solution by high energy ball milling. *Powder Technol* 214:117–121
- Williamson GK, Hall WH (1953) X-ray line broadening from filed aluminium and wolfram. *Acta Metall* 1:22–31
- Khakpour Z, Youzbashi AA, Maghsoudipour A, Ahmadi K (2012) Electrical behavior of Gd-doped CeO_2 electrolyte ceramics sintered from nano powders prepared by mechanical alloying process. *J Mater Sci Mater Electron* 23:786–794
- Zhang TS, Ma J, Kong LB, Hing P, Leng YJ, Chan SH, Kilner JA (2003) Sinterability and ionic conductivity of co precipitated $Ce_{0.8}Gd_{0.2}O_{2-\delta}$ powders treated via a high-energy ball-milling process. *J Power Sources* 124:26
- Aoki M, Chiang YM, Kosachi I, Lee LIR, Tuller H, Liu YP (1996) Solute segregation and grain-boundary impedance in high-purity stabilized zirconia. *J Am Ceram Soc* 79:1169–1180
- Guo X, Waser R (2006) Electrical properties of the grain boundaries of oxygen ion conductors: acceptor-doped zirconia and ceria. *Prog Mater Sci* 51:151–210
- Mori T, Kobayashi T, Wang Y, Drennan J, Nishimura T, Li JG, Kobayashi H (2005) Synthesis and characterization of nano-heterostructured Dy doped CeO_2 solid electrolytes using a combination of spark plasma sintering and conventional sintering. *J Am Ceram Soc* 88:1981–1984
- Jiang SP, Love JG, Badwal SPS (1997) Electrochemical techniques in studies of solid ionic conductors. *Key Eng Mater* 125–126:81–132
- Esposito V, Traversa E (2008) Design of electroceramics for solid oxides fuel cell applications: playing with ceria. *J Am Ceram Soc* 91: 1037–1051
- Yamamura H, Katoh E, Ichikawa M, Kakinuma K, Mori T, Haneda H (2000) Multipledoping effect on the electrical conductivity in the $(Ce_{1-x-y}La_xM_y)O_{2-\delta}$ ($M = Ca, Sr$) system. *Electrochemistry* 455–459

44. Kim DJ (1989) Lattice parameters, ionic conductivities, and solubility limits in fluorite-structure MO_2 oxide [$\text{M} = \text{Hf}^{4+}, \text{Zr}^{4+}, \text{Ce}^{4+}, \text{Th}^{4+}, \text{U}^{4+}$] solid solutions. *J Am Ceram Soc* 72:1415–1421
45. Lee JH, Mori T, Li JG, Ikegami T, Komatsu M, Haneda H (2000) Improvement of grain-boundary conductivity of 8 mol% yttria-stabilized zirconia by precursor scavenging of siliceous phase. *J Electrochem Soc* 147:2822–2829
46. Lee JH, Mori T, Li JG, Ikegami T, Drennan J, Kim DY (2002) Precursor scavenging of resistive grain-boundary phase in 8 mol% yttria-stabilized zirconia. *J Electrochem Soc* 149:J35–J40